Received: 19 October 2019 | Revised: 10 November 2019 | Accepted: 17 November 2019

DOI: 10.1002/inf2.12072

REVIEW ARTICLE

WILEY

Two-dimensional materials: From mechanical properties to flexible mechanical sensors

Hanjun Jiang[1,2] | **Lu Zheng**[1,2] | **Zheng Liu**[4,5,6] | **Xuewen Wang**[1,3]

[1]Institute of Flexible Electronics, Northwestern Polytechnical University, Xi'an, China

[2]MIIT Key Laboratory of Flexible Electronics (KLoFE), Northwestern Polytechnical University, Xi'an, China

[3]Shaanxi Key Laboratory of Flexible Electronics (KLoFE), Northwestern Polytechnical University, Xi'an, China

[4]School of Materials Science and Engineering, Nanyang Technological University, Singapore

[5]Centre for Micro-/Nano-electronics (NOVITAS), School of Electrical & Electronic Engineering, Nanyang Technological University, Singapore

[6]CINTRACNRS/NTU/THALES, Research Techno Plaza, Singapore

Correspondence
Zheng Liu, School of Materials Science and Engineering, Nanyang Technological University, Singapore.
Email: z.liu@ntu.edu.sg

Xuewen Wang, Institute of Flexible Electronics, Northwestern Polytechnical University, Xi'an, 710072, China.
Email: iamxwwang@nwpu.edu.cn

Funding information
Fundamental Research Funds for the Central Universities, Grant/Award Numbers: 31020190QD010, 3102019PY004, 3102019JC004; Ministry of Education - Singapore, Grant/Award Numbers: MOE2015-T2-2-043, MOE2017-T2-2-136, Tier 1 RG7/18; National Natural Science Foundation of China, Grant/Award Number: 11904289; Natural Science Foundation of Shaanxi Province, Grant/Award Number: 2019JQ-613; Start-up funds from Northwestern Polytechnical University, Grant/Award Numbers: 19SH020159, 19SH020123

Abstract

Two-dimensional (2D) materials have great potential in the fields of flexible electronics and photoelectronic devices due to their unique properties derived by special structures. The study of the mechanical properties of 2D materials plays an important role in next-generation flexible mechanical electronic device applications. Unfortunately, traditional experiment models and measurement methods are not suitable for 2D materials due to their atomically ultrathin thickness, which limits both the theoretical research and practical value of the 2D materials. In this review, we briefly summarize the characterization of mechanical properties of 2D materials by in situ probe nanoindentation experiments, and discuss the effect of thickness, grain boundary, and interlayer interactions. We introduce the strain-induced effect on electrical properties and optical properties of 2D materials. Then, we generalize the mechanical sensors based on various 2D materials and their future potential applications in flexible and wearable electronic devices. Finally, we discuss the state of the art for the mechanical properties of 2D materials and their opportunities and challenges in both basic research and practical applications.

KEYWORDS

2D materials, flexible mechanical sensor, mechanical property, strain effect

1 | INTRODUCTION

Atomically thin two-dimensional (2D) materials have attracted a large amount of attention in the past few years due to their unique and excellent electric, optical, magnetic, and mechanical properties since graphene was obtained successfully by micromechanical cleavage from graphite in 2004.[1] As a monolayer atomic carbon of crystal, graphene has shown high thermal conductivity (3000-5000 W m^{-1} K^{-1}), an excellent optical transparency

of 98%,[2] and an extremely high Young's modulus of 1 TPa.[3] Meanwhile, it can bear strains of more than 25% without fracture.[3] Beyond graphene, other atomic thin-layered 2D nanomaterials such as transition metal dichalcogenides (TMDs) were investigated widely. As the most presentative TMDs, monolayer MoS_2 shows Young's modulus as high as 270 GPa,[4] which is equal to that of steel. Monolayer MoS_2 crystal manifests a direct bandgap of 1.9 eV, while bulk MoS_2 is a semiconductor with an indirect bandgap of about 1.2 eV.[5,6] Monolayer WS_2 also shows a strong photoluminescence (PL) intensity.[7] The flexural stiffness of materials is proportional to the cube of its thickness. Therefore, a decrease in the thickness of materials could improve the flexibility of materials by decreasing flexural stiffness. 2D nanomaterials with atomic thickness could sustain a small radius of curvature, which make them possess a natural advantage for the construction of flexible electronics. All these unique features of atomic thickness 2D materials make them great potential applications in the next generation of flexible, slight, and transparent electronic and optoelectronic devices, such as wearable health-monitoring devices, flexible energy storage devices, and collapsible intelligent screens.

In order to promote the practical applications of these materials, we must have a full understanding of the physical and chemical properties of them, for there are still many mysterious properties of 2D materials unknown. For example, mechanical property plays an important role in multitudinous physical properties of 2D materials, and it is also an essential part of the manufacture of devices. However, studies on the mechanical property of 2D materials only occupy a small amount of the whole 2D materials family up to now.[8,9] There are mainly two reasons that caused the present situation. The atomically ultrathin thickness of 2D crystals is different from metals, organic polymers, or some kinds of other traditional materials, the result that cannot fit a traditional mature experimental model of mechanical property test. For another, the experiment technique such as syntheses of kinds of high-quality and large-scale 2D materials is still a big challenge. Until now, some of the papers have reviewed the synthesis, mechanical, and electrical properties, as well as applications of 2D materials separately, but in this review, we combined mechanical properties and their effects on the electrical properties of 2D materials, and discussed how these features affected their flexible mechanical sensor applications.

In this article, we summarize the nanoindentation characterization experiments of freely suspended 2D materials from fabrication to measurement of mechanical properties. The electrical and optical properties of 2D materials, such as electronic state, band energy, PL, and Raman shift, are discussed when strain is applied to the materials by stretching or bending the substrate. Finally, we generalize flexible mechanical sensors based on graphene and other 2D materials, especially the wearable sensors for monitoring physiological signals toward human health.

2 | NANOINDENTATION OF FREELY SUSPENDED 2D MATERIALS

2.1 | Theoretical modules

Testing the mechanical properties of 2D materials is difficult by traditional stretching and bending method because small grain size and special thickness of 2D materials down to atomic thin, which is hard to bring precise strain impact to 2D materials. Probe microscopy technique provides an effective way to measure and operate the low-dimensional materials at the nanoscale. The nanoprobe was employed to apply the tiny pressure to materials at a specific location, which could be fixed at the nanoarea. The technique could be used to investigate the deformation of 2D materials at the sub-nanoscale by measurement of the deformation of the cantilever. Besides the experimental method, scientists also devoted to characterizing the mechanical properties of 2D materials by theoretical calculation, such as molecular dynamics simulations,[10,11] first-principles calculations,[12] and density functional theory (DFT).[13]

To date, the most widely used model for the mechanical properties of 2D materials is the suspended circular drum model (Figure 1A) and the doubly-clamped beam model (Figure 1D).[9,18] Both two models require 2D materials that should be suspended partially onto the substrate and provide the degree of freedom for the deformation of 2D materials in the vertical direction. Figure 1A shows a 2D nanofilm deposited on a porous SiO_2 substrate. The sample can attach to the substrate around the hole firmly by van der Waals' interactions. Therefore, the material above the hole is in a stretched state and does not collapse, which provides the center of the suspended part of 2D material for pressure applying by an atomic force microscopy (AFM) probe. The schematic of the AFM-based nanoindentation test for acquiring force-deformation behaviors is shown in Figure 1F. For continuum mechanics model, the relationship between the load and the deformation of AFM tip can be expressed as follows[17]:

$$F = \left[\frac{4\pi E}{3(1-\nu^2)}\cdot\left(\frac{t^3}{R^2}\right)\right]\delta + (\pi T)\delta + \left(\frac{q^3 E t}{R^2}\right)\delta^3, \quad (1)$$

where F represents the applied force, δ is the deformation of the sample, E is the elastic modulus, t is the thickness of the material, R is the radius of the hole, and T is the

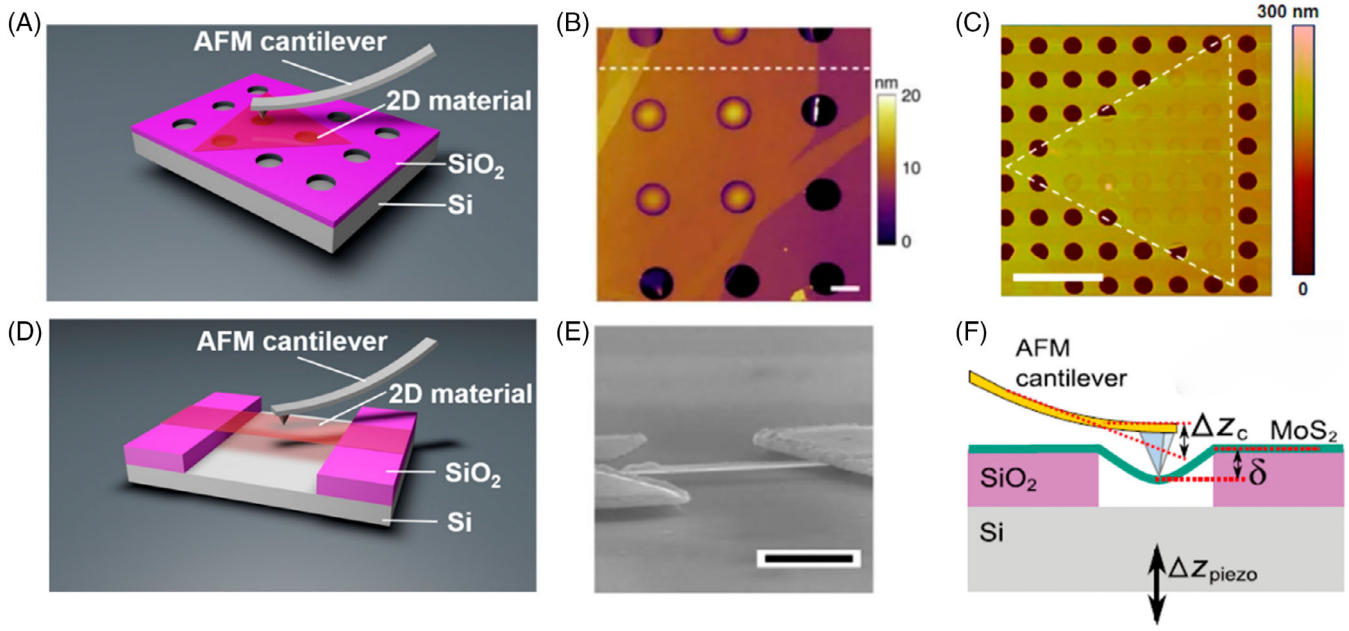

FIGURE 1 Schematic diagram of AFM nanoindentation characterization and freely suspended 2D material. A, Freely-suspended circular drum model. B, AFM topography of exfoliated monolayer BN flake on porous SiO_2/Si substrate. Reproduced with permission.[14] Copyright 2017, Nature Publishing Group. C, AFM image of CVD-grown monolayer MoS_2 transferred onto the SiO_2/Si substrate. Reproduced with permission.[15] Copyright 2014, American Chemical Society. D, Freely suspended doubly-clamped beam model. E, SEM image from different views of two $NbSe_2$ films on the SiO_2/Si substrate. Reproduced with permission.[16] Copyright 2010, American Physical Society. F, Schematic of the AFM-based nanoindentation test for acquiring F(δ) behaviors. Reproduced with permission.[17] Copyright 2012, Wiley-VCH. Scale bars: B,E, 1 μm; C, 5 μm

pretension in the film. ν is the Poisson's ratio, q is a constant, and q can be represented by ν, $q = 1/(1.05 - 0.15\nu - 0.16\nu^2)$. In Equation (1), the first term describes the mechanical behavior of a circular bending plate, the second part takes into account the pretension of film, and the last term is essential for thin membrane under large deformation. The equation could be used to analyze and establish elastic modulus and pretension from the F–δ curve.

The breaking strength of the sample can be determined by increasing the load force of AFM tip until flakes produce the fracture. The related equation was given by Bertolazzi et al[4]:

$$\sigma_m^{2D} = \sqrt{\frac{FE^{2D}}{4\pi R}}, \tag{2}$$

where σ_m^{2D} is the maximum stress of the center point, F is the force at the breaking point, E^{2D} is the 2D modulus, and the quotient of E^{2D} and thickness is the elastic modulus of the flakes. σ_m^{2D} can represent the intrinsic strength when the materials possess the perfect crystal structure without defect. Therefore, this equation can help investigate the effect of defect distribution and grain size on the quality of 2D crystals by comparing their fracture behavior.

A schematic illustration of the doubly-clamped beam is described as in Figure 1B. The process of characterization is similar to the drum. The F–δ curve can be expressed by Li et al[19]:

$$F = \frac{Ew\pi^4}{6}\left(\frac{t}{l}\right)^3\delta + \frac{w\sigma_0\pi^2}{2}\left(\frac{t}{l}\right)\delta + \frac{Ew\pi^4}{8}\left(\frac{t}{l^3}\right)\delta^3, \tag{3}$$

where l is the length of the beam, w and t is the width and thickness of the film, respectively, and σ_0 is the pretension. E of the beam could be determined by F–δ curve in Equation (3). Similar to Equation (1), the first term in Equation (3) represents the linear elastic behavior of the bending beam. The second term is attributed to the pretension of the stretched beam, and the third term takes into account the beam under large deformation. The doubly-clamped has a limitation on the measurement of breaking strength, which is different from the circular drum model.

The above two strategies were widely used to investigate the elastic property, intrinsic strength, and bending rigidity of graphene,[3] MoS_2,[4,17,20] boron nitride (BN),[14,21] $MoTe_2$,[22] and black phosphorus (BP).[23] Despite impressive

progress in the mechanical properties study of 2D materials, there are still challenges in the accurate characterization of mechanical properties for partial 2D materials like $MoTe_2$.[22] It is also challenging to acquire freely suspended chemical vapor deposition (CVD)-grown $MoTe_2$ and WTe_2 because they are unstable and decompose within several minutes in the air. On the other hand, defects in materials, such as grain boundary, will have an impact on their mechanical behavior during testing experiments. Therefore, the fabrication of freely suspended crystals with high quality is crucial for the investigation of mechanical properties of 2D materials.

2.2 | Fabrication of freely suspended 2D material

In order to measure the mechanical properties of 2D materials by nanoindentation experiment, freely suspended 2D materials were fabricated by the following two strategies:

2.2.1 | Transferring

First, there is transfer of 2D materials onto prepatterned substrates with an array of holes or trenches.[24-29] The flowchart of fabrications of freely suspended 2D materials is shown in Figure 2A. Firstly, a patterned substrate with microcavity should be prepared by micromanufacturing such as UV lithography and electron beam lithography. The resolution of the micromachining technique can reach to the nanometer scale, which is smaller than the size of most 2D materials that ranged in the microscale. Therefore, those preparing microholes/nanoholes are used to make suspending 2D films. Also, considering the size and radius (ranging 20-100 nm) of AFM tip for nanoindentation test, the diameter of holes and the width of trenches are usually designed between 0.5 and 3 μm. Figure 1B shows an optical microscopy image of freely suspended monolayer BN flake on a SiO_2 substrate with an array of holes.[14] The researchers prepared a porous SiO_2/Si substrate by a UV photolithography process and then etched the substrate to form hole patterns with a size of 1.3 μm in diameter. The scotch tape with exfoliated BN flakes was pressed onto the substrate and peeled it slowly. BN flakes could attach to the substrate by van der Waals force. The breaking strength and interlayer interaction of layered BN with different thicknesses (1-9 layers) were investigated. A similar method was also utilized in MoS_2,[20] graphene,[25] BP,[23] and Mica.[26] However, this method has limitations due to the uncontrollable thickness and low yield by mechanical exfoliation. It is also challenging to obtain monolayer crystal with a large size. CVD has been widely used in controllable syntheses of various 2D materials like MoS_2[30] and WS_2.[31,32] Therefore, transferring CVD grown to patterned substrates is a feasible way to fabricate freely suspended samples.[33,34]

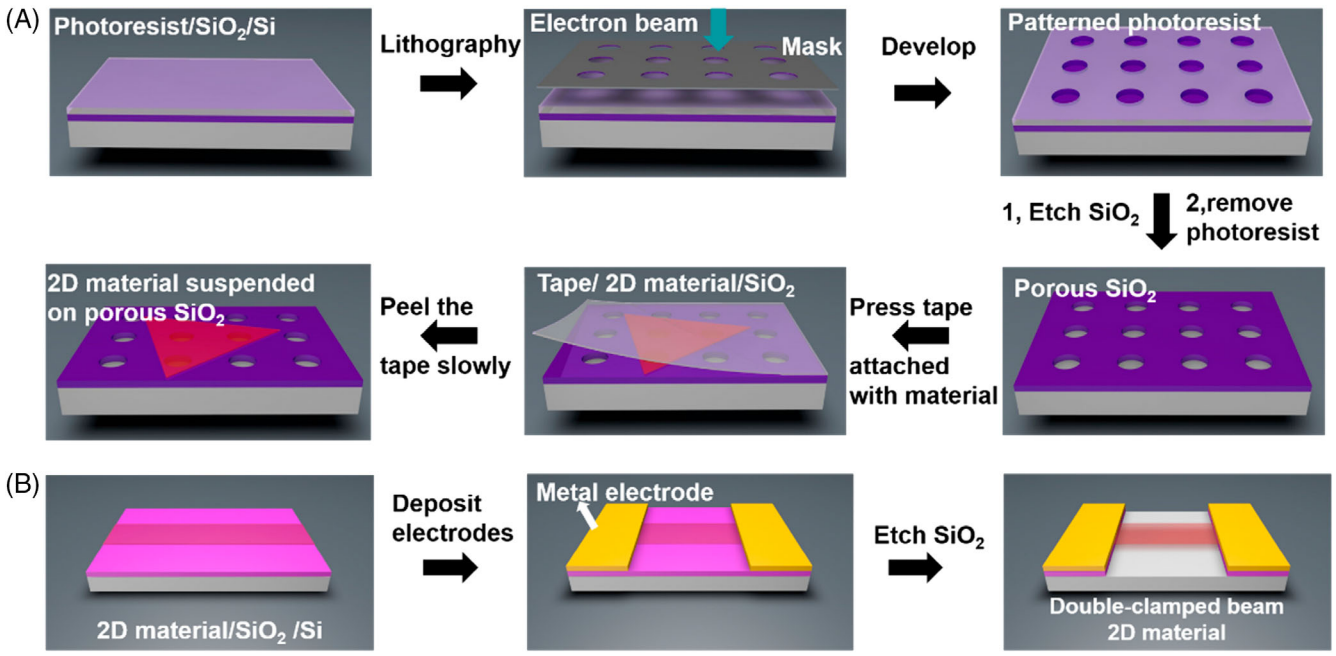

FIGURE 2 Schematic illustration of fabrication of freely suspended 2D material. A, Freely suspended circular drum model. B, Freely suspended doubly-clamped beam model

Figure 1C shows an AFM image of CVD grown MoS_2 on porous SiO_2/Si substrate.[15] Liu et al. synthesized MoS_2 by CVD on a smooth substrate and transferred the nanosheets to a porous SiO_2/Si substrate assisted by poly(methyl methacrylate) and polydimethylsiloxane (PDMS). This method possesses a high success rate. However, chemical reagents such as potassium hydroxide and acetone were used to lift off 2D materials to target substrates in this process, which could bring damage to materials.

2.2.2 | Depositing followed by etching

In this method, deposition of 2D materials onto smooth substrates takes place and then etching part of the substrate under the samples.[16,35-38] Figure 2B shows the schematic illustration of fabrication. The first step of this strategy is transferring flakes by CVD or mechanical exfoliation on a smooth substrate. Then metal electrodes were fabricated on the sides of 2D materials. Finally, part of the substrate under the samples was etched away by buffered oxide etchant. Figure 1E shows the scanning electron microscopy (SEM) image of freely suspended $NbSe_2$ nanosheet on SiO_2/Si substrate.[16] This method is widely used to fabricate a doubly-clamped beam structure and investigate the dynamic electromechanical signal of electronic devices. It is important to note that the drying process should be careful to avoid the collapse due to the surface tensile effect.[19]

Both of the above methods are not a universal one that could be applied to all of the 2D materials. Therefore, it is important to select the appropriate method for different materials. Fabrication of freely suspended 2D materials is vital to carry out a nanoindentation experiment by an AFM probe for investigating their mechanical properties. In addition, the abovementioned process on SiO_2 substrate can also be improved for application of the flexible substrate.

2.3 | In situ probe characterization

2.3.1 | Elastic property and breaking strength of intrinsic 2D materials

Based on the double-clamped beam model and the suspended circular drum model, many studies on the mechanical property of 2D materials have been carried out by AFM tip nanoindentation in the past 10 years. Lee et al[3] investigated Young's modulus and breaking strength of the exfoliated single-layer graphene flakes. The force-deformation curve (Figure 3A) shows a nonlinear elastic stress-strain behavior with an extremely high value of $E = 1.0$ TPa. Figure 3B shows the fracture loads of graphene with different tip radii and film diameters, and the result indicated an extremely high intrinsic strength that could reach up to 130 GPa for the defect-free graphene, which demonstrated that the graphene is the strongest material in the world.

Beyond graphene, the mechanical properties of other 2D materials such as TMDs,[4,17] BN,[14] BP,[23] and tungsten nitride (WN)[39] have been measured. Wang et al synthesized the high crystalline WN and Young's modulus of the WN is about 390 GPa, which is the best value except graphene and hBN reported previously.[39] Simone et al studied the stretching and bending behaviors of free-standing monolayer and few-layers MoS_2 nanosheets by nanoindentation measurements.[4] It is revealed that the average Young' modulus of monolayer MoS_2 samples is 270 $\pm$100 GPa, which is comparable to the steel. The high breaking strength of monolayer MoS_2 is up to 22 $\pm$4 GPa, corresponding to a highly effective strain of 6-11%. The maximal breaking limitation by theoretical calculation of monolayer MoS_2 is 10%, which indicated that the strongest membrane crystal possessed high quality and almost no defect. Besides, few layered MoS_2 flakes from 5 to 25 layers have demonstrated that the bending stiffness and thickness of 2D materials are positive correlations.[17] As shown in Figure 3C, the force-deformation curves exhibited a nonlinear to linear behavior from 5 to 20 layers, which is consistent with graphene that reported previously.[40] Combined with the mechanical strength, controllable bandgap, and excellent optical performances, graphene and TMDs such as MoS_2 and WS_2 manifest great potential in the flexible semiconductor photoelectric devices.

2.3.2 | The role of grain boundary and interlayer interactions

Expect for single-crystal 2D materials, polycrystalline and heterostructure of 2D materials with lots of grain boundaries have been studied to explain how grain boundaries and interactions between interlayers affect the mechanical property of 2D materials. Figure 4A gives single MoS_2 crystal and a polycrystalline continues MoS_2 nanofilm with grain boundaries in it. Li et al synthesized large-scale hBN by CVD and investigated the elastic property and fracture behavior of different flakes with various defect distributions.[21] Figure 4C gives the calculated strain energy of hBN with different defect concentrations. As shown in Figure 4D, the breaking strain of hBN is not related to the defect concentration, which is different from the stress concentration caused by microcracks. It

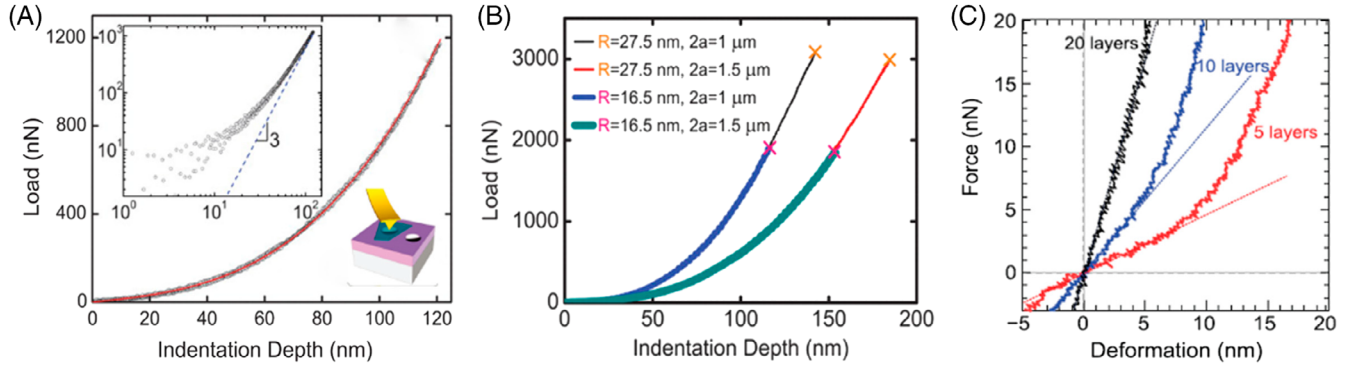

FIGURE 3 Force-deformation curves of 2D materials based on AFM nanoindentation experiment. A, Force-deformation curve of exfoliated freely suspended graphene. B, Fracture load of graphene with different tip radii (R) and film diameters (2a). × is the fracture point. A,B, Reproduced with permission.[3] Copyright 2008, Science Publishing Group. C, Force-deformation curve (nonlinear to linear behavior) of exfoliated freely suspended MoS_2 with 5, 10, and 20 layers by experiment. Reproduced with permission.[17] Copyright 2012, Wiley-VCH

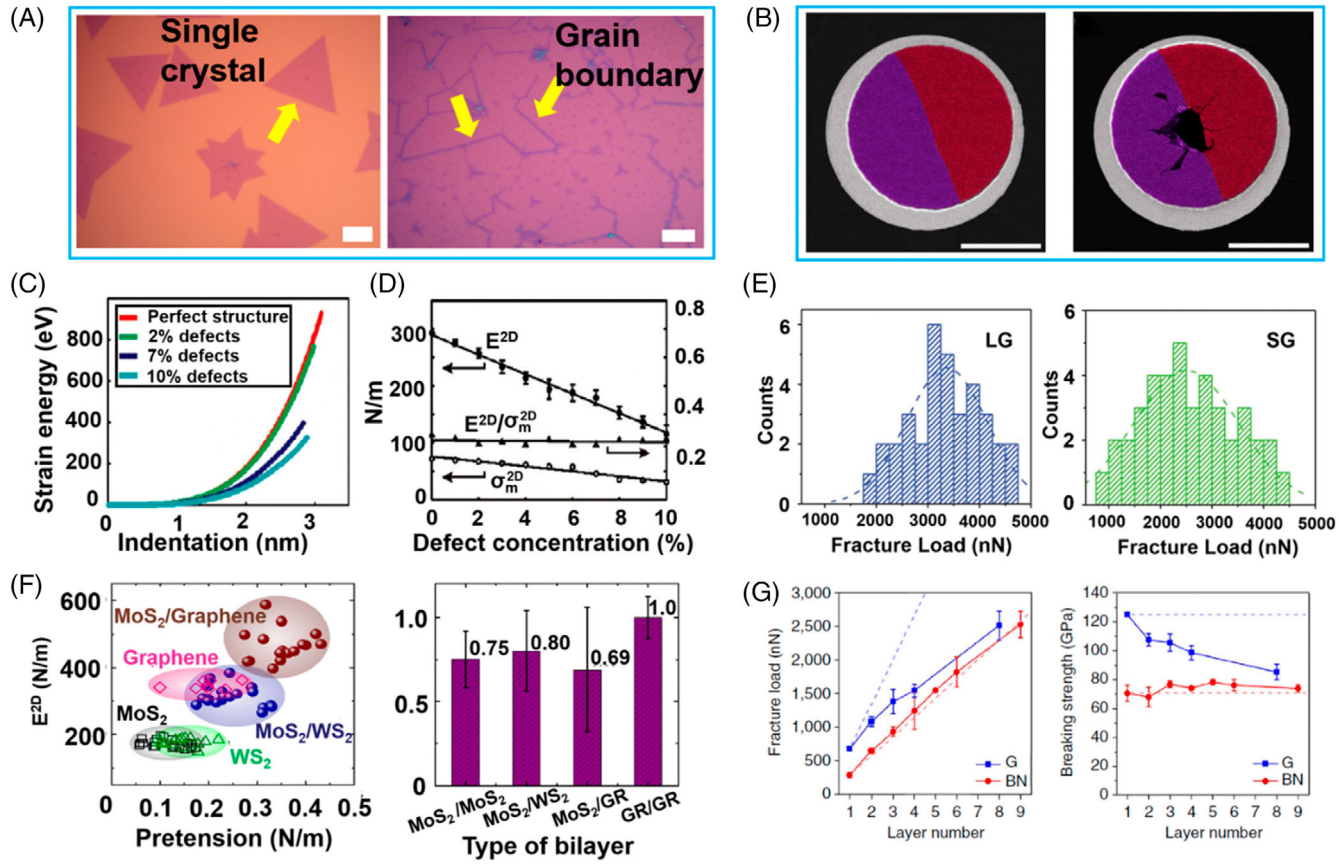

FIGURE 4 Grain boundary effect and interlayer interactions of 2D materials. A, Optical image of single MoS_2 crystal and continuous polycrystalline MoS_2 film. Grain boundaries in polycrystalline MoS_2 were pointed by the yellow arrow. B, Composite false-color DF-TEM image of a bicrystal graphene membrane before and after fracture measurement. Reproduced with permission.[41] Copyright 2013, Nature Publishing Group. C, The strain energy of the BN sheet as a function of the indentation depth for different defect concentrations. Inset, BN nanofilm on the Si substrate. D, The dependence of 2D modulus (E^{2D}), breaking stress (σ_m^{2D}), and breaking strain (ε) on the defect concentration. Reproduced with permission.[21] C,D, Copyright 2010, American Chemical Society. E, Fracture loads of single crystal graphene with large grain (LG) and continuous graphene film with a small grain (SG). Reproduced with permission.[42] Copyright 2013, Science Publishing Group. F, E^{2D} and interaction coefficient of different bilayer heterostructure. Reproduced with permission.[15] Copyright 2014, American Chemical Society. G, Fracture loads and breaking strength of BN (red, 1-9 layers) and graphene (blue, 1-8 layers). Reproduced with permission.[14] Copyright 2017, Nature Publishing Group. Scale bars: A, 10 μm; B, 500 nm

has been suggested that the out-of-plane wrinkles could decrease the in-plane stiffness significantly, and the existence of grain boundaries of polycrystalline could effectively weaken the fracture strength of graphene films.[43] Rasool and coworkers[41] reported that the low-angle grain boundaries could reduce the strength of graphene nanosheets. However, polycrystalline graphene membranes with large-angle grain boundaries incarnated the comparative intrinsic strength to the single crystalline by mechanical exfoliation technique. It can be explained by the sub-nanostrain effect in the C—C covalent bonds at the boundary. Lee et al[42] explored the impact of grain size on elastic property and strength of graphene nanofilms fabricated by CVD. Figure 4B shows false-color, dark-field transmission electron microscopy (DF-TEM) images of the same bicrystal graphene membrane before and after fracture induced by AFM nanoprobe. The results show that the elastic stiffness of continuous polycrystalline membranes with small grains (SG) is comparable to that of single graphene crystal with a large grain (LG). Besides, as shown in Figure 4E, the intrinsic strength of SG graphene with grain boundaries is only 10% lower than LG graphene. Therefore, the large-size polycrystalline 2D material possesses competitive strength to pristine materials, suggesting that it could be the best candidate applied in flexible and bendable devices.

The interlayer interaction of few-layered or multilayered 2D materials and heterojunction have also been studied. Lots of investigations demonstrated that the interlayer interaction varies in a wide range for graphene, BN,[14] MoS_2,[15] and platinum disulfide (PtS_2).[44] Liu et al[15] investigated the bilayer heterojunction combined with CVD-grown MoS_2 as the bottom layer and exfoliated WS_2 as the top layer. The results show that the 2D modulus of MoS_2/WS_2 heterojunction is 314 ± 31 N m^{-1}, which is not equal to the sum of each layer (171 ± 11 N m^{-1} for MoS_2, 177 ± 12 N m^{-1} for WS_2). The above results were caused by weak interaction and sliding effects between layers. Figure 4F gives the 2D modulus and interaction coefficients of different heterostructures. The interaction coefficients range from 0.69 to 0.8, indicating a weak interlayer coupling for bilayer MoS_2/MoS_2, MoS_2/WS_2, and MoS_2/graphene. However, the few-layered BN obtained by mechanical exfoliation exhibited a completely different conclusion.[14] Figure 4G gives a comparison of the breaking strength of graphene and BN with different layers. It is confirmed that the intrinsic strength for BN with different thicknesses from 1 to 9 layers is approximative, which revealed a strong interaction between layers under large deformation. Taking into account their high performance on thermal stability, layered BN could be a good choice for mechanical reinforcement. The properties of Young's modulus and intrinsic strength for 2D materials are summarized in Table 1. In general, Young' modulus of most 2D materials is between 150 and 400 GPa, and they exhibit an effective strain of about 10%. The inherent diversity of 2D materials and different interlayer interactions make their mechanical strength vary in a broad range. Therefore, 2D materials with different properties and regulate heterostructures were selected to meet the specific requirements in practice applications.

3 | STRETCHING AND BENDING OF 2D MATERIALS

3.1 | Stretching and bending behavior of 2D materials on the flexible substrate

The mechanical strain such as stretching and bending could change the atomic structure of 2D materials, effecting lattice vibration, electronic structure, bandgap, and thermal conductivity, which result in a diversification of their electrical, optional, and magnetic properties.[53,54] Recent literature studies have reported that monolayer graphene could withstand 25% strain without structural breaking.[3] The remarkable mechanical characteristics provide a great foundation for strain-induced studies of 2D materials. As shown in Figure 5A,B, substrate-induced strain refers to applying a load on a stretchable or bendable substrate attached with 2D material so that a small strain could be induced into 2D material from the deformed substrate via the van der Waals attractions between the substrate and material. It was a common way to apply stretch and stress to 2D materials for investigation of their strain effects.

Several strategies could increase the strain in 2D materials and provide an excellent way for the substrate-induced strain regulation research and preparation technology for flexible wearable electronic devices. Zhang et al[55] studied the substrate-induced behaviors of WS_2 crystal on a PDMS substrate. Figure 5C,D has shown the morphology of single WS_2 crystal under different strains in optical and AFM images. The effective strain transfer rates are about 12% when the substrate tensile strain is below 0.16. Wrinkles were produced due to strain relaxation of WS_2 when the strain of PDMS ranges from 0.16 to 0.32. Besides, as shown in Figure 5E,F, wrinkled MoS_2 could be fabricated by depositing it on a pre-stretched PDMS substrate and released the tension in the substrate suddenly.[56] A similar transfer efficiency of ~10% was obtained in CVD-grown MoS_2 deposited on a PDMS substrate without a relative slide between the samples and tensile substrate.[57] The strain transfer efficiency is limited

TABLE 1 Young's modulus and intrinsic strength of 2D materials

2D materials	Elastic modulus (GPa)	Breaking strength (GPa)	Method	Reference
MoS_2	270 ± 100	23	Nanoindentation	4
	210	26.8	DFT	27
	185		Nanoindentation	19
	330 ± 70		Nanoindentation	17
	300		Nanoindentation	20
2H $MoTe_2$	110 ± 16	5.6 ± 1.3	Nanoindentation	22
1T' $MoTe_2$	99 ± 15	2.6 ± 0.2	Nanoindentation	22
Graphene oxide	207.6 ± 23.4		Nanoindentation	45
Vermiculite	175 ± 16		Nanoindentation	46
BN	865 ± 73	70.5 ± 5.5	Nanoindentation	14
	276 ± 32.4	25	Nanoindentation	23
	58.6 ± 11.7	4.79 ± 1.43	Nanoindentation	47
WN	390 ± 160		Nanoindentation	39
Graphene	1000	130	Nanoindentation	3
	500	30	Nanoindentation	48
	1120		Nanoindentation	24
	250		Nanoindentation	35
	~1100		MM	10
		112	FEM	49
	890		Nanoindentation	50
Mica	190		Nanoindentation	26
WSe_2	167.3 ± 6.7	12.4	Nanoindentation	51
Bi_2Se_3	17.86–25.45		Nanoindentation	52
Bi_2Te_3	11.7–25.7		Nanoindentation	34

by the weak van der Waals interaction, and it could be improved to 60% by selecting high modulus substrate (~650 MPa).[57] In addition, Yang et al[58] pointed out that the curing process of PDMS could enhance the adhesion of 2D materials to the substrate and generate a uniaxial tensile strain of exfoliated MoS_2 sheets by bending the flexible substrate. Apart from the experimental research, the response of 2D materials attached to the flexible substrate could also be studied by theoretical simulation.[59,60]

3.2 | Electrical properties under strain

Recent studies have demonstrated that electrical properties, including band structure, conductivity, and mechanical properties like elasticities, are thickness dependent and structural dependent in 2D materials such as MoS_2 and WS_2. Therefore, electrical properties and performance could be regulated of 2D materials by structure changing resulting from applied mechanical strain. There are many studies on electrical and mechanical interactions that have been carried out to investigate the change of electronic structure and bandgap of 2D materials based on strain effect.

Strain-induced bandgap engineering has been a research hotspot and is of great significance to regulate the bandgap of 2D layered semiconductors. Figure 6A is a schematic diagram of the uniaxial tensile experiment and optical characterization of MoS_2/PDMS structure. The electric structure of monolayer MoS_2 under different strains based on DFT calculation is shown in Figure 6D. The red arrows mark a specific band and it is the conduction band minimum when compressive strain was applied, but it increased above the conduction band minimum without strain or in a tensile state. Andres Castellanos-Gomez and co-workers[56] demonstrated that the local high strain region of MoS_2 with uniform wrinkles has an apparent decrease of the bandgap and exciton trapping. The PL spectra of the wrinkled region show obvious red-shift compared to that of flat MoS_2, and the direct bandgap transition changes about −90 meV when the tensile strain increased to about 2.5%. Moreover,

TABLE 2 Flexible mechanical sensors based on 2D materials and their performance

2D materials	Type of sensor	Detection range	(Measurement range) sensitivity	Response time	Reference
Mxene	Pressure sensor	10.2 Pa~30 kPa	(23–982 Pa) 0.55 kPa^{-1}	11 ms	[91]
			(982–10 kPa) 3.81 kPa^{-1}		
			(10–30 kPa) 2.52 kPa^{-1}		
α-Bi_2Se_3	Strain sensor		GF~237		[77]
GaSe	Strain sensor		(0%–20%) GF~−4.3		[93]
GO/rGO	Pressure sensor	Max 450 kPa	0.002 kPa−1	200 ms	[89]
rGO	Strain sensor	0.1%–400%	(0.1%–1%) GF~2.5	60 ms	[94]
			(390%–400%) GF~31.6		
	Pressure sensor	Max 87 kPa	0.122 kPa^{-1}		[94]
rGO	Pressure sensor	Min 9 Pa	(0–10 kPa) 0.26 kPa^{-1}		[87]
Gr	Pressure sensor	Max 2000 kPa	(0–1000 kPa) 0.09 kPa^{-1}	100 ms	[86]
	Strain sensor		(0%–18%) GF~2.6		[86]
			(22%–40%) GF~8.5		
Gr	Strain sensor	Max 30%	(0%–0.2%) GF~2.6		[85]
			(2%–6%) GF~10^3		
			(More than 7%) GF~10^6		
Gr	Pressure sensor	0~60 kPa	0.122 kPa^{-1}		[88]
	Strain sensor		(0%–1.5%) GF~43		[88]
Gr	Pressure sensor	Min 1 Pa	(0–12 kPa) 8.5 kPa^{-1}	40 ms	[79]
MoS_2	Strain sensor	Max −5.23%	(−1.98%–0%) GF~72.5		[90]
			(0%–1.98%) GF~56.5		
MoS_2	Pressure sensor	1–120 kPa	0.011 kPa^{-1}	180 ms	[78]

Abbreviations: GF, gauge factor; GO, graphene oxide; Gr, graphene; rGO, reduced graphene oxide.

there is a nearly linear monotonically decreasing relationship between the bandgap and applied strain of MoS_2 within a specific range.[61] He et al[64] studied the change of bandgap of MoS_2 with different layers on an elastomeric substrate, for the direct bandgap of MoS_2 has a red-shift at a rate of 70 meV/% tensile strain and the indirect bandgap is about 110 meV/% strain. Figure 6C gives the PL peak energy of trilayer MoS_2 nanofilm under an increasing compressive strain from 0 to 0.2%,[62] and the linear fit result of the experiment demonstrated the band energy increased at a rate of 300 meV per percent biaxial compressive strain. Besides, the mechanical strain could convert the band structure of WS_2/MoS_2 from direct to indirect bandgap.[61,65] Theoretical studies by first-principles calculations also identified the abovementioned experimental results, and it confirmed that strain-induced electrical effect is not only limited to MX_2 (M = Mo, W; X = S, Se, Te),[63] but also in BP,[60] graphene, and other 2D materials.[54]

Apart from the bandgap structure affected by strain, piezoelectricity is another crucial strain-induced electrical property for layered 2D materials, especially for monolayer materials with nonsymmetrical structure.[66-69] Figure 7A,B gives the atom structure and mechanism of piezoelectricity of monolayer MoS_2. The high quality of the crystal, low bending stiffness, and the tolerance for large strain of 2D materials make them great potential in flexible piezoelectric applications such as highly sensitive flexible mechanical sensors and precise actuators with atomic resolution. Figure 7E shows a flexible device based on monolayer MoS_2 nanosheets and high performance on mechanical-to-electrical conversion by stretching and releasing it repeatedly, with an output of ~15 mV and ~20 pA under 0.53% strain. However, a completely different phenomenon was observed in bilayer and bulk samples.[66] The piezoelectricity of intrinsic even-layer and bulk 2D materials disappears due to the absence of a noncentrosymmetric structure. However, Lee et al[67] fabricated a different crystal orientation bilayer WSe_2 by transferring the CVD-grown single-layer WSe_2 twice and stack them (tb-WSe_2) on the PET substrate. Surprisingly, as shown in Figure 7F, reliable piezoelectricity was observed in the flexible nanogenerators composed by bilayer WSe_2 and PET substrate under a

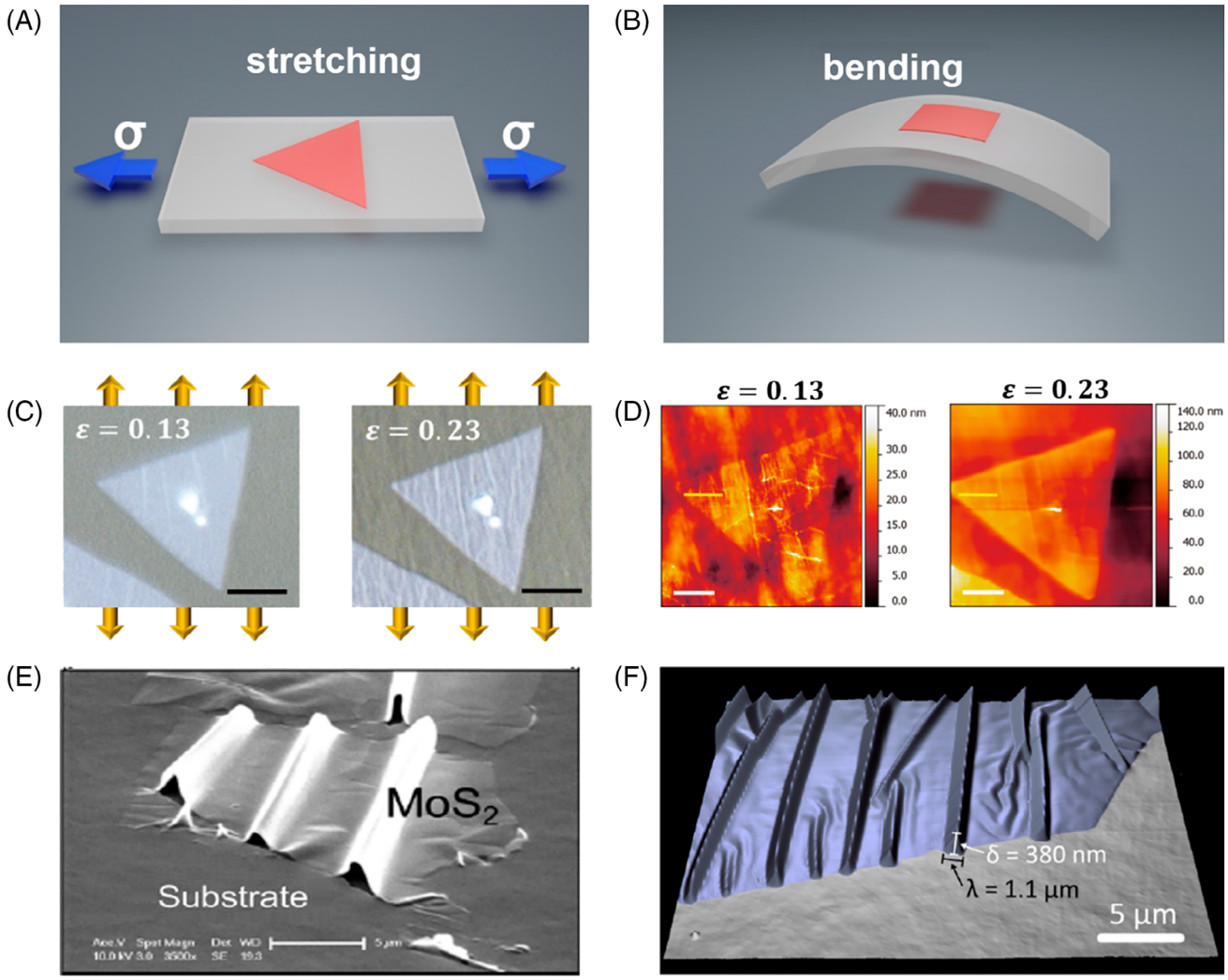

FIGURE 5 Substrate-induced strain in 2D materials. A,B, Schematic diagram of stretching and bending models of flexible substrate attached with 2D materials. The red part is the 2D materials, the white part is the stretchable or bendable substrate, and the blue arrow is the direction of the applied load. C, Optical images of the tensile strain effect on the morphology of WS_2 crystal on the PDMS substrate. The strain values are given on PDMS.[55] D, AFM images of the same crystal in C. Copyright 2016, Wiley-VCH. E, SEM image of wrinkled MoS_2.[56] F, AFM image of a wrinkled on PDMS substrate.[56] Copyright 2013, American Chemical Society. Scale bars: C,E, 5 μm; D, 3 μm

tensile strain by bending the component. Furthermore, flexible optoelectronics based on MoS_2[68] and MoS_2/WSe_2 heterojunction[69] were also fabricated and tested. The MoS_2-based device illustrated an ultrahigh photoresponsivity of 2.3×10^4 A W^{-1}, which was 26 times higher than that of the best value from monolayer MoS_2 optoelectronics reported previously. As shown in Figure 7H, the photocurrents changed apparently under different strains at the same illumination intensity, indicating that the device could be an effective strain-gated photodetector. Piezoelectricity of 2D materials provides a novel idea and strategy for high-performance flexible piezoelectric devices, such as highly sensitive flexible mechanical sensors and precise actuators with atomic resolution.

3.3 | Optical properties under strain

The strain effect of 2D materials is also related to the lattice vibration and crystal orientation, resulting in the change of optical properties such as PL and Raman shift.[71] It is well known that the diversification of bandgap and light emission energy is owing to the electronic configuration and energy levels based on the change of atomic structure by applied strain. Many scientists were devoted to understanding how the lattice vibrations mode of 2D materials is affected by the strain.

Recently, strain-induced optical properties of graphene, TMDs, and phosphorene have been investigated by both experimental practice and theoretical predictions. Wang et al[72] studied the strain-induced lattice vibrations and

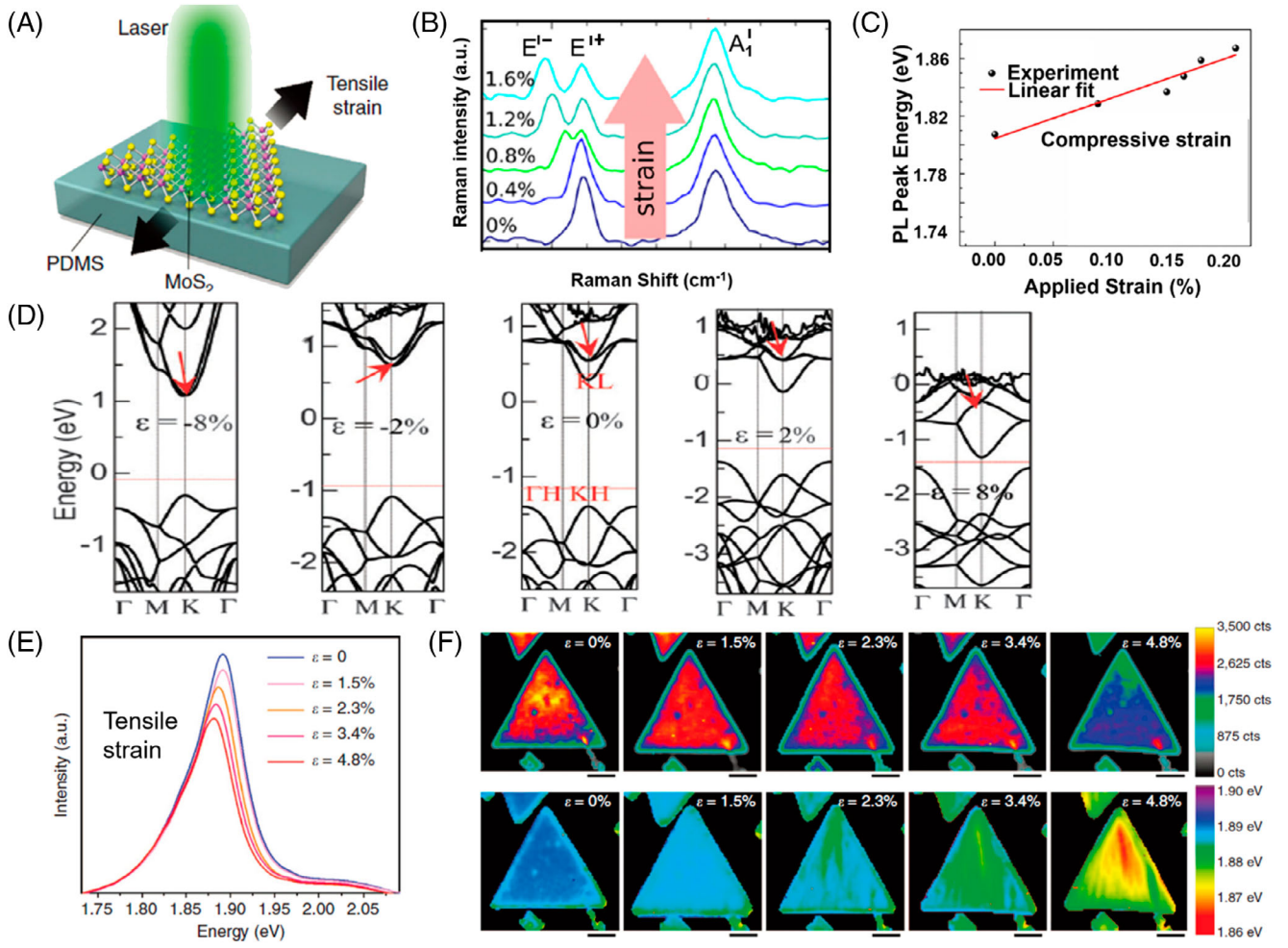

FIGURE 6 Strain effects on bandgap and Raman shift of MoS_2. A, Schematic diagram of uniaxial tensile experiment and optical characterization of MoS_2/PDMS structure. Reproduced with permission.[57] Copyright 2014, Nature Publishing Group. B, Raman shift of monolayer MoS_2 as strained from 0% to 1.6%. The peak of E^1_{2g} mode split into two peaks with increasing strain. Reproduced with permission.[61] Copyright 2013, American Chemical Society. C, Photoluminescence peak energy of trilayer MoS_2 under compressive strain from 0% to 0.2%. Reproduced with permission.[62] Copyright 2013, American Chemical Society. D, Electric structure of monolayer MoS_2 under different strains based on density functional theory calculation, −8%, −2%, 0%, 2%, and 8%, respectively. The red arrow marks a specific band. It is the conduction band minimum under compressive strain, but changed when no strain or tensile strain was applied. The red line is the Fermi level. Reproduced with permission.[63] Copyright 2012, Royal Society of Chemistry. E, PL spectra of monolayer MoS_2 under an increasing tensile strain from 0% to 4.8%. F, PL intensity and peak position mapping under the same strain from E. E,F, Reproduced with permission.[57] Copyright 2014, Nature Publishing Group

crystallographic orientation of exfoliated monolayer MoS_2 flakes attached to PET by exerting a uniaxial tensile strain on the flexible substrate. As shown in Figure 6B, Raman shift revealed that the in-plane A_{1g} vibration mode is not sensitive to the strain while the out-plane E^1_{2g} changed apparently. More specifically, the E^1_{2g} mode showed a palpable red-shift within 1.0% strain, which means they soften phonon modes and lower frequency caused by the larger twofold degeneracy, and it gradually split into two peaks due to the damaged symmetry lattice beyond 1% strain. A similar phenomenon and conclusion of monolayer WS_2[65] and MoS_2[73,74] were confirmed by the first-principles calculations. Yang et al[58] pointed out that the in-plane tensile strain of multilayer MoS_2 (more than six layers) could lead to obvious blue-shift of E^1_{2g} due to the stronger interlayer van der Waals force. Correspondingly, the out-of-plane tensile strain could reduce the vibration frequency of both E^1_{2g} and A_{1g} modes in multilayer MoS_2 due to the weakened interlayer interactions.

Expect for TMDs, the strain effects on lattice vibrations and phonon modulations of phosphorene[60] and graphene[59,75] were investigated by theoretical calculation, and they also exhibited a significant change of Raman shift and vibration frequency. The strain-dependent optical and electronic properties of 2D materials expand their applications of flexible nano-optoelectronic devices.

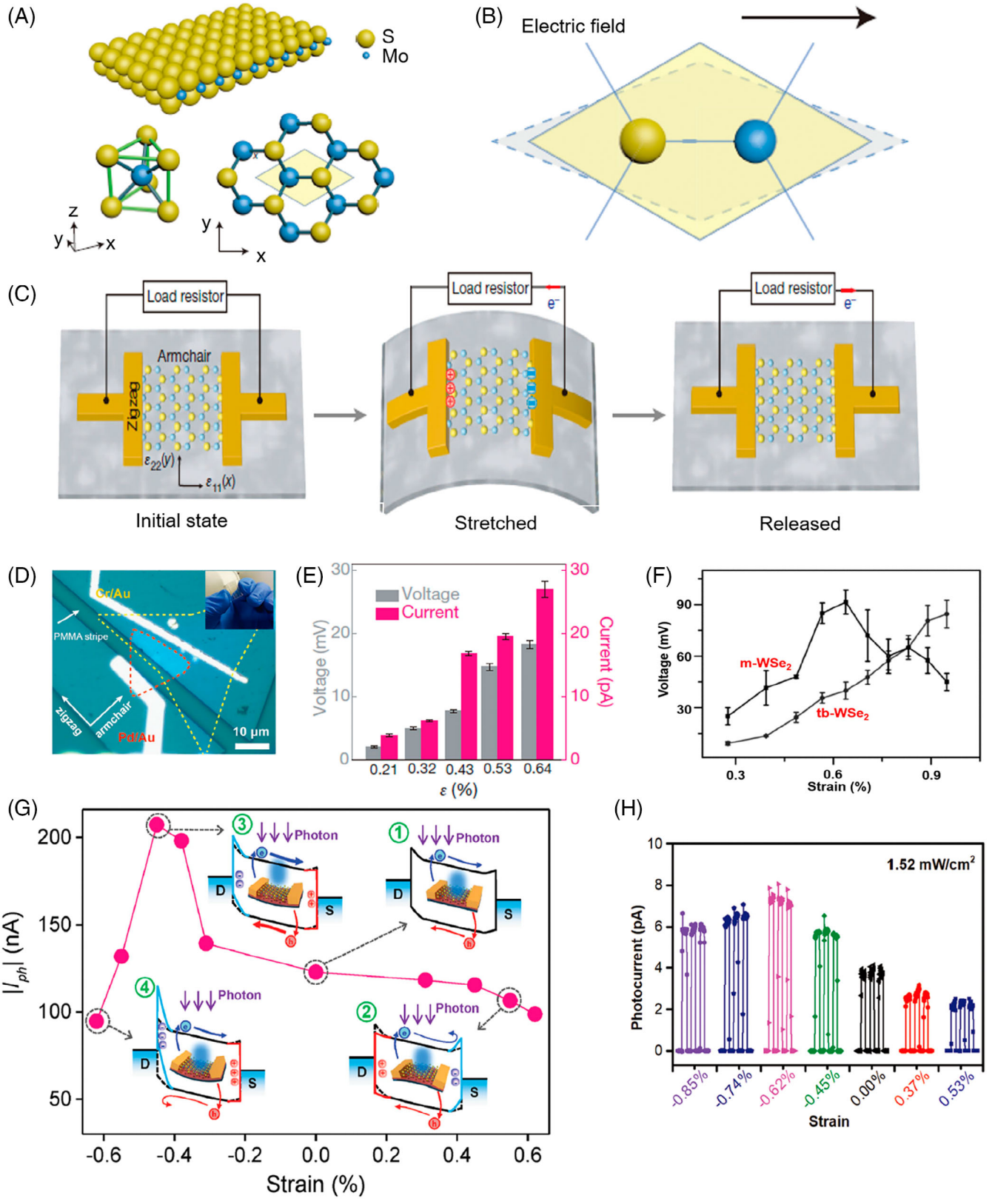

FIGURE 7 Legend on next page.

4 | FLEXIBLE MECHANICAL SENSOR APPLICATION

The excellent mechanical and electrical properties of 2D materials such as extremely low bending rigidity and tunable bandgap endow them the best candidate for next-generation flexible electronics, which could be used in wearable health-monitoring devices, biocompatible electric skins, a flexible display, and artificially intelligent robots. Figure 8 gives several flexible sensor applications based on 2D materials for human health.[77,79-81] Herein, we highlight the flexible mechanical sensors, including strain sensors, pressure sensors, and vibration sensors, with high performance on sensitivity, lightweight, portable, durable, and low energy consumption. A flexible strain sensor based on In_2Se_3[77] and a large-sized active-matrix MoS_2[78] tactile sensor array are shown in Figure 8B. Typically, the mechanical sensors are composed of conducting sensing materials, flexible electrode, and stretchable or bendable substrate (eg, Ecoflex, PDMS, PET, PI).

In recent years, graphene-based flexible sensors have attracted much attention and exhibit unprecedented performance with high sensitivity (161.6 kPa^{-1} within 0.56 kPa),[82] long-term stability (50 000 cycles),[83] and low response time (11 ms).[84] Wang et al[85] synthesized graphene woven fabrics on flexible PMDS and medical tape substrate to fabricate the graphene-PDMS-medical tape-based strain sensor by piezoresistive-type configuration. The sensor performed high sensitivity in the detection of slight human motions such as the wrist pulse, respiration, and eyes blink. It possessed a high gauge factor (GF) of ~35 under a small deformation of 0.2% and ~10^3 under 2%-6% strains. At the same time, it exhibited good reversibility even under a large strain of 30%. Such a type of flexible sensor is ultrasensitive to the various kinds of sound signals, including the different Chinese characters; English letters; phrases and animal sounds from dog, bird, cow, and horse,[80] exhibiting huge potential to the acquisition and identification of large amounts of sundry audio information for the digital signal processing.

Structural design and engineering of materials have been demonstrated that play an important role in enhancing the performances of flexible sensors.[79,86,87] For example, Bae et al[79] developed transparent electronic skin by a bionic structure with high-quality monolayer graphene that covered entirely on PDMS substrate with a hierarchically distributed architecture array. The sensor has shown a high sensitivity of 8.5 kPa^{-1}, swift response time of 40 ms, and low detection limit of only 1 Pa, which makes it can be used to detect the pulse precisely. Besides, the sensor exhibited reliable stability after 10 000 cycles of testing, which is an important factor in practical applications. Yao et al[87] designed a graphene-polyurethane sponge with high pressure-sensitive property based on fractured microstructure. The study recovered that modulus of the flexible substrate, the intrinsic resistance of graphene,[79] and the form and size of graphene flakes[88] have a notable impact on the GF of flexible sensors. Chen[88] proposed to improve the sensitivity of flexible sensors by adding the sodium deoxycholate to graphene ink. The GF was improved by more than 50% because the surfactant molecules could enhance the tunneling barrier width of graphene film and make it more sensitive to interlayer motion.

The above sensors are only able to monitor the single signal, which limits their practice application severely in wearable biomedical electronic devices. Ho and co-workers integrated the multifunctional sensors by stacking the different sensor units together via a lamination process. The integrated sensor arrays are capable of detecting the humidity, thermal conductivity, and pressure simultaneously.[89] Each unit of the sensor is only impressible to the particular stimulation and do not interact and crosstalk each other. The strategy of integration enables artificial E-skin to detect multiple physiological signals simultaneously.

FIGURE 7 Piezoelectricity and piezophototronic effects of TMDs. A, Diagram of the atomic structure of monolayer MoS_2. The bottom left and bottom right are the side view and top view, respectively. B, With an external electric field pointing from the S site to the Mo site, the Mo-2S dipole is stretched and the unit cell is elongated. A,B, Reproduced with permission.[70] Copyright 2014, Nature Publishing Group. C, Schematic diagram of the piezoelectric device on flexible substrate. Reproduced with permission.[66] Copyright 2014, Nature Publishing Group. D, Optical image of flexible p-n photodiode device based on MoS_2/WSe_2 heterostructure and metal electrodes at its edges. The yellow and red dotted lines represent MoS_2 and WSe_2, respectively. Reproduced with permission.[69] Copyright 2018, Wiley-VCH. E, External strain dependence of the voltage and current outputs of monolayer MoS_2-based piezoelectric device. Reproduced with permission.[66] Copyright 2014, Nature Publishing Group. F, Voltages output as a function of applied strain in piezoelectric devices based on m-WSe_2 (monolayer WSe_2) and tb-WSe_2 (bilayer WSe_2 by stacking two monolayer WSe_2 randomly). Reproduced with permission.[67] Copyright 2017, Wiley-VCH. G, Piezophototronic response mechanism of a strain-dependent monolayer MoS_2 flexible device. Reproduced with permission.[68] Copyright 2016, Wiley-VCH. H, Photocurrent of MoS_2/WSe_2 photodiode under different applied strain values in the same illumination. Reproduced with permission.[69] Copyright 2018, Wiley-VCH

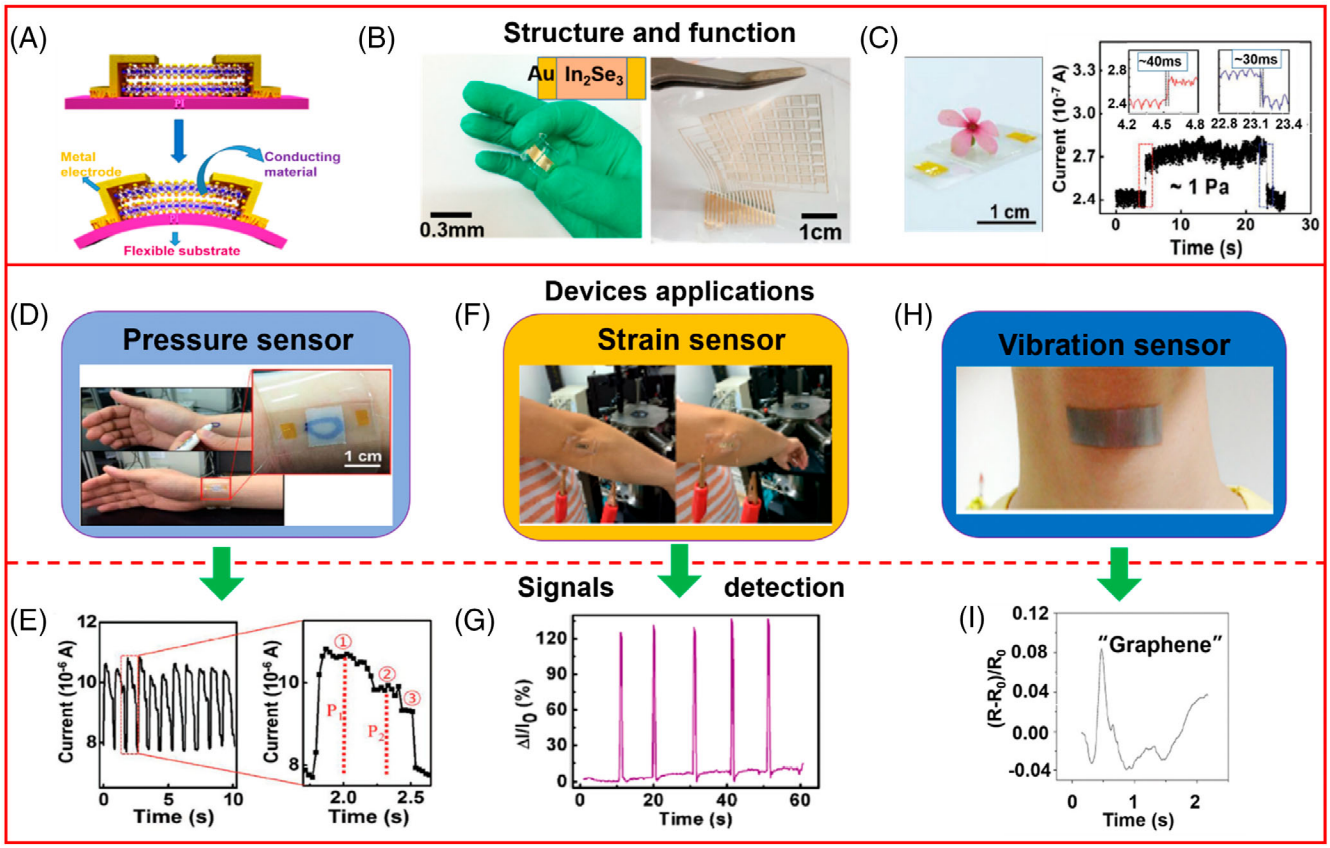

FIGURE 8 Flexible sensors based on 2D materials. A, Schematic of flexible mechanical sensor based on 2D materials and flexible substrate. Reproduced with permission.[76] Copyright 2019, American Chemical Society. B, left panel) Photograph of a flexible strain sensor based on In_2Se_3. right panel). Optical image of a large-scale active-matrix MoS_2 tactile sensor array. Reproduced with permission.[77,78] Copyright 2016, American Chemical Society. Copyright 2019, American Chemical Society. C, Optical image of a pressure sensor based on graphene under a light flower (about 1 Pa) and current output. Reproduced with permission.[79] D,E, A pressure sensor attached to the wrist and pulse signal response. Reproduced with permission.[79] Copyright 2016, Wiley-VCH. F,G, A strain sensor to test the signal caused by endow bending and corresponding electrical response. Reproduced with permission.[77] Copyright 2016, American Chemical Society. H, A vibration sensor attached to the throat to detect sound signals. I, Recognition of "graphene" in H. H,I, Reproduced with permission.[80] Copyright 2014, Springer Science

Beyond the graphene-based sensors, kinds of other 2D materials were also investigated widely for the mechanical sensors, such as MoS_2,[90] MXene,[91] α-In_2Se_3,[77] and MoS_2/graphene.[92] Park et al[90] employed bilayer MoS_2 as the active materials to produce large-scale tactile sensors. The results indicated that the change of resistance could reach up to 3.24% when the applied strain is 0.24% and it can keep initial property even bending for 10 000 cycles, indicating the high sensitivity and good stability. Due to the excellent conductivity and large specific surface area, the porous nanostructured MXene shows a fast response time of 11 ms, a low detection limit to 10.2 Pa, and excellent stability after 10 000 cycles.[91] The performance of flexible mechanical sensors based on 2D materials was summarized as Table 2. All these sensors and E-skin with great performance approve that various 2D materials are a favorable candidate for the new-generation flexible mechanical sensor. The sensor based on CVD-grown MoS_2 has exhibited a relatively high GF than that of conventional metal and silicon sensors; however, the performance is not as good as that of strain sensor fabricated by exfoliated single crystalline MoS_2 due to the defect and small grain size of material, which illustrated that the growth of large-scale crystal with high quality is critical for the development of sensor devices.

5 | CONCLUSION AND OUTLOOK

The exploration of elastic properties, stiffness, the effect of grain size and defect, strain engineering, and flexible mechanical sensors of 2D materials have attracted tremendous interest in the past few years. The present studies proved that layered 2D nanomaterials with atomic

thickness possess high surface-to-volume ratio and excellent mechanical strength and electrical conductivity. Due to the morphology and unique properties of 2D materials, the electronic and optoelectronic devices based on 2D materials are lightweight, miniature, and energy saving, which meet the demands of the specific applications in the field of aerospace and wearable electronic devices. In addition, diverse 2D materials have exhibited versatile and unprecedented physical properties in many different aspects. Combined with evolving integrated processes, 2D materials will bring endless possibilities on multifunctional and intelligent device applications. They are definitely the most suitable candidate for next-generation flexible electronic evolution, including electro-mechanical sensors, biomedical devices, energy storage, field effect transistors, supercapacitors and so on.

It should be clearly understood that the cognition of various 2D materials is still in an early stage. So there are both changes and challenges at the same time in the fundamental research and practical applications. The large-scale 2D materials such as graphene and TMDs have been synthesized by CVD, while the grain boundaries and defect make them at a disadvantage compared with exfoliated flakes from bulk. In addition, despite considerable achievements in the characterization of mechanical properties based on nanoindentation, the uncontrollable factors such as damage to samples during the complicated preparation and testing process have a nonnegligible influence on the result. In the future, searching for new 2D materials and fabrication of 2D crystals at a large scale and of high quality, more precise calculating methods and reasonable experimental models for characterization, measurement, and advanced device fabrication technology are still vital for the studies of ultrathin 2D nanomaterials.

ACKNOWLEDGMENTS

L. Zheng and H. Jiang contributed equally to this work. This work is supported by the Fundamental Research Funds for the Central Universities (3102019P Y004, 31020190QD010, 3102019JC004), the National Natural Science Foundation of China (11904289), the Natural Science Foundation of Shaanxi Province (2019JQ-613), and start-up funds from Northwestern Polytechnical University (19SH020159, 19SH020123). This work is also supported by MOE Tier 1 RG7/18, MOE2015-T2-2-043 and MOE2017-T2-2-136.

ORCID

Zheng Liu https://orcid.org/0000-0002-8825-7198
Xuewen Wang https://orcid.org/0000-0002-9689-6678

REFERENCES

1. Novoselov KS, Geim AK, Morozov SV, et al. Electric field effect in atomically thin carbon films. *Science*. 2004;306(5696):666-669.
2. Yang HG, Xue TY, Li FY, Liu WT, Song YL. Graphene: diversified flexible 2D material for wearable vital signs monitoring. *Adv Mater Technol*. 2019;4(2):1800574.
3. Lee C, Wei XD, Kysar JW, Hone J. Measurement of the elastic properties and intrinsic strength of monolayer Graphene. *Science*. 2008;321(5887):385-388.
4. Bertolazzi S, Brivio J, Kis A. Stretching and breaking of ultrathin MoS_2. *ACS Nano*. 2011;5(12):9703-9709.
5. Mak KF, Lee C, Hone J, Shan J, Heinz TF. Atomically thin MoS_2: a new direct-gap semiconductor. *Phys Rev Lett*. 2010;105(13):136805.
6. Splendiani A, Sun L, Zhang Y, et al. Emerging photoluminescence in monolayer MoS_2. *Nano Lett*. 2010;10(4):1271-1275.
7. Gutierrez HR, Perea-Lopez N, Elias AL, et al. Extraordinary room-temperature photoluminescence in triangular WS_2 monolayers. *Nano Lett*. 2013;13(8):3447-3454.
8. Akinwande D, Brennan CJ, Bunch JS, et al. A review on mechanics and mechanical properties of 2D materials—Graphene and beyond. *Extreme Mech Lett*. 2017;13:42-77.
9. Castellanos-Gomez A, Singh V, van der Zant HSJ, Steele GA. Mechanics of freely-suspended ultrathin layered materials. *Ann Phys Berlin*. 2015;527(1-2):27-44.
10. Ni ZH, Bu H, Zou M, Yi H, Bi KD, Chen YF. Anisotropic mechanical properties of graphene sheets from molecular dynamics. *Physica B*. 2010;405(5):1301-1306.
11. Zhou LX, Xue JM, Wang YG, Cao GX. Molecular mechanics simulations of the deformation mechanism of graphene monolayer under free standing indentation. *Carbon*. 2013;63:117-124.
12. Duan WH, Wang CM. Nonlinear bending and stretching of a circular graphene sheet under a central point load. *Nanotechnology*. 2009;20(7):075702.
13. Xiong S, Cao G. Bending response of single layer MoS_2. *Nanotechnology*. 2016;27(10):105701.
14. Falin A, Cai Q, Santos EJG, et al. Mechanical properties of atomically thin boron nitride and the role of interlayer interactions. *Nat Commun*. 2017;8:15815.
15. Liu K, Yan Q, Chen M, et al. Elastic properties of chemical-vapor-deposited monolayer MoS_2, WS_2, and their bilayer heterostructures. *Nano Lett*. 2014;14(9):5097-5103.
16. Sengupta S, Solanki HS, Singh V, Dhara S, Deshmukh MM. Electromechanical resonators as probes of the charge density wave transition at the nanoscale in$NbSe_2$. *Phys Rev B*. 2010;82(15):155432.
17. Castellanos-Gomez A, Poot M, Steele GA, van der Zant HS, Agrait N, Rubio-Bollinger G. Elastic properties of freely suspended MoS_2 nanosheets. *Adv Funct Mater*. 2012;24(6):772-775.
18. Cao GX, Gao HJ. Mechanical properties characterization of two-dimensional materials via nanoindentation experiments. *Prog Mater Sci*. 2019;103:558-595.
19. Li P, You Z, Cui TH. Molybdenum disulfide dc contact MEMS shunt switch. *J Micromech Microeng*. 2013;23(4):045026.
20. Castellanos-Gomez A, Poot M, Steele GA, van der Zant HSJ, Agraït N, Rubio-Bollinger G. Mechanical properties of freely suspended semiconducting graphene-like layers based on MoS_2. *Nanoscale Res Lett*. 2012;7(1):233.
21. Song L, Ci L, Lu H, et al. Large scale growth and characterization of atomic hexagonal boron nitride layers. *Nano Lett*. 2010;10(8):3209-3215.

22. Sun YF, Pan JB, Zhang ZT, et al. Elastic properties and fracture Behaviors of Biaxially deformed, polymorphic $MoTe_2$. *Nano Lett*. 2019;19(2):761-769.
23. Wang JY, Li Y, Zhan ZY, Li T, Zhen L, Xu CY. Elastic properties of suspended black phosphorus nanosheets. *Appl Phys Lett*. 2016;108(1):013104.
24. Annamalai M, Mathew S, Jamali M, Zhan D, Palaniapan M. Elastic and nonlinear response of nanomechanical graphene devices. *J Micromech Microeng*. 2012;22(10):105024.
25. Bunch JS, van der Zande AM, Verbridge SS, et al. Electromechanical resonators from Graphene sheets. *Science*. 2007;315 (5811):490-493.
26. Castellanos-Gomez A, Poot M, Amor-Amorós A, et al. Mechanical properties of freely suspended atomically thin dielectric layers of mica. *Nano Res*. 2012;5(8):550-557.
27. Cooper RC, Lee C, Marianetti CA, Wei XD, Hone J, Kysar JW. Nonlinear elastic behavior of two-dimensional molybdenum disulfide. *Phys Rev B*. 2013;87(3):035423.
28. Garcia-Sanchez D, van der Zande AM, Paulo AS, Lassagne B, McEuen PL, Bachtold A. Imaging mechanical vibrations in suspended Graphene sheets. *Nano Lett*. 2008;8(5):1399-1403.
29. Wong CL, Annamalai M, Wang ZQ, Palaniapan M. Characterization of nanomechanical graphene drum structures. *J Micromech Microeng*. 2010;20(11):115029.
30. He TY, Li YJ, Zhou ZF, et al. Synthesis of large-area uniform MoS_2 films by substrate-moving atmospheric pressure chemical vapor deposition: from monolayer to multilayer. *2D Mater*. 2019;6(2):025030.
31. Zafar A, Zafar Z, Zhao WW, et al. Sulfur-mastery: precise synthesis of 2D transition metal Dichalcogenides. *Adv Funct Mater*. 2019;29(27):1809261.
32. Zhou JD, Lin JH, Huang XW, et al. A library of atomically thin metal chalcogenides. *Nature*. 2018;556(7701):355-359.
33. Suk JW, Kitt A, Magnuson CW, et al. Transfer of CVD-grown monolayer Graphene onto arbitrary substrates. *ACS Nano*. 2011;5(9):6916-6924.
34. Guo L, Yan H, Moore Q, et al. Elastic properties of van der Waals epitaxy grown bismuth telluride 2D nanosheets. *Nanoscale*. 2015;7(28):11915-11921.
35. Gómez-Navarro C, Burghard M, Kern K. Elastic properties of chemically derived single Graphene sheets. *Nano Lett*. 2008;8 (7):2045-2049.
36. Lindahl N, Midtvedt D, Svensson J, et al. Determination of the bending rigidity of graphene via electrostatic actuation of buckled membranes. *Nano Lett*. 2012;12(7):3526-3531.
37. Shivaraman S, Barton RA, Yu X, et al. Free-standing epitaxial Graphene. *Nano Lett*. 2009;9(9):3100-3105.
38. Traversi F, Javier Gúzman-Vázquez F, Giorgia Rizzi L, et al. Elastic properties of graphene suspended on a polymer substrate by e-beam exposure. *New J Phys*. 2010;12(2):023034.
39. Wang H, Sandoz-Rosado EJ, Tsang SH, et al. Elastic properties of 2D ultrathin tungsten nitride crystals grown by chemical vapor deposition. *Adv Funct Mater*. 2019;29(31):1902663.
40. Poot M, van der Zant HSJ. Nanomechanical properties of few-layer graphene membranes. *Appl Phys Lett*. 2008;92(6): 063111.
41. Rasool HI, Ophus C, Klug WS, Zettl A, Gimzewski JK. Measurement of the intrinsic strength of crystalline and polycrystalline graphene. *Nat Commun*. 2013;4(1):2811.
42. Lee G-H, Cooper RC, An SJ, et al. High-strength chemical-vapor-deposited Graphene and grain boundaries. *Science*. 2013; 340(6136):1073-1076.
43. Ruiz-Vargas CS, Zhuang HL, Huang PY, et al. Softened elastic response and unzipping in chemical vapor deposition graphene membranes. *Nano Lett*. 2011;11(6):2259-2263.
44. Zhao YD, Qiao JS, Yu P, et al. Extraordinarily strong interlayer interaction in 2D layered PtS_2. *Adv Mater*. 2016;28(12):2399-2407.
45. Suk JW, Piner RD, An J, Ruoff RS. Mechanical properties of monolayer Graphene oxide. *ACS Nano*. 2010;4(11):6557-6564.
46. Suk JW, Piner RD, An J, Ruoff RS. Evaluation of elastic modulus of ultra-thin vermiculite membranes by contact mode atomic force microscopy imaging. *Thin Solid Films*. 2013;527: 205-209.
47. Tao J, Shen WF, Wu S, et al. Mechanical and electrical anisotropy of few-layer black phosphorus. *ACS Nano*. 2015;9(11): 11362-11370.
48. Frank IW, Tanenbaum DM, van der Zande AM, McEuen PL. Mechanical properties of suspended graphene sheets. *J Vac Sci Technol B*. 2007;25(6):2558-2561.
49. Niu TX, Cao GX, Xiong CY. Fracture behavior of graphene mounted on stretchable substrate. *Carbon*. 2016;109:852-859.
50. Zhang YP, Pan CX. Measurements of mechanical properties and number of layers of graphene from nano-indentation. *Diam Relat Mater*. 2012;24:1-5.
51. Zhang R, Koutsos V, Cheung R. Elastic properties of suspended multilayer WSe_2. *Appl Phys Lett*. 2016;108(4):042104.
52. Yan H, Vajner C, Kuhlman M, et al. Elastic behavior of Bi_2Se_3 2D nanosheets grown by van der Waals epitaxy. *Appl Phys Lett*. 2016;109(3):032103.
53. Lu X, Luo X, Zhang J, Quek SY, Xiong Q. Lattice vibrations and Raman scattering in two-dimensional layered materials beyond graphene. *Nano Res*. 2016;9(12):3559-3597.
54. Amorim B, Cortijo A, de Juan F, et al. Novel effects of strains in graphene and other two dimensional materials. *Phys Rep*. 2016;617:1-54.
55. Zhang QH, Chang ZY, Xu GZ, et al. Strain relaxation of monolayer WS_2 on plastic substrate. *Adv Funct Mater*. 2016;26(47): 8707-8714.
56. Castellanos-Gomez A, Roldán R, Cappelluti E, et al. Local strain engineering in atomically thin MoS_2. *Nano Lett*. 2013;13 (11):5361-5366.
57. Liu Z, Amani M, Najmaei S, et al. Strain and structure heterogeneity in MoS_2 atomic layers grown by chemical vapour deposition. *Nat Commun*. 2014;5(1):5246.
58. Yang L, Cui XD, Zhang JY, et al. Lattice strain effects on the optical properties of MoS_2 nanosheets. *Sci Rep UK*. 2014;4:5649.
59. Ma F, Zheng HB, Sun YJ, Yang D, Xu KW, Chu PK. Strain effect on lattice vibration, heat capacity, and thermal conductivity of graphene. *Appl Phys Lett*. 2012;101(11):111904.
60. Fei RX, Yang L. Lattice vibrational modes and Raman scattering spectra of strained phosphorene. *Appl Phys Lett*. 2014;105 (8):083120.
61. Conley HJ, Wang B, Ziegler JI, Haglund RF, Pantelides ST, Bolotin KI. Bandgap engineering of strained monolayer and bilayer MoS_2. *Nano Lett*. 2013;13(8):3626-3630.
62. Hui YY, Liu XF, Jie WJ, et al. Exceptional tunability of band energy in a compressively strained trilayer MoS_2 sheet. *ACS Nano*. 2013;7(8):7126-7131.

63. Lu P, Wu X, Guo W, Zeng XC. Strain-dependent electronic and magnetic properties of MoS_2 monolayer, bilayer, nanoribbons and nanotubes. *Phys Chem Chem Phys*. 2012;14(37):13035-13040.
64. He K, Poole C, Mak KF, Shan J. Experimental demonstration of continuous electronic structure tuning via strain in atomically thin MoS_2. *Nano Lett*. 2013;13(6):2931-2936.
65. Wang YL, Cong CX, Yang WH, et al. Strain-induced direct-indirect bandgap transition and phonon modulation in monolayer WS_2. *Nano Res*. 2015;8(8):2562-2572.
66. Wu WZ, Wang L, Li YL, et al. Piezoelectricity of single-atomic-layer MoS_2 for energy conversion and piezotronics. *Nature*. 2014;514:470-474.
67. Lee J-H, Park JY, Cho EB, et al. Reliable piezoelectricity in bilayer WSe_2 for piezoelectric Nanogenerators. *Adv Mater*. 2017;29(29):1606667.
68. Wu WZ, Wang L, Yu RM, et al. Piezophototronic effect in single-atomic-layer MoS_2 for strain-gated flexible optoelectronics. *Adv Mater*. 2016;28(38):8463-8468.
69. Lin P, Zhu LP, Li D, Xu L, Pan CF, Wang ZL. Piezo-Phototronic effect for enhanced flexible MoS_2/WSe_2 van der Waals photodiodes. *Adv Funct Mater*. 2018;28(35):1802849.
70. Zhu HY, Wang Y, Xiao J, et al. Observation of piezoelectricity in free-standing monolayer MoS_2. *Nat Nanotechnol*. 2014;10:151-155.
71. Ren HT, Xiong ZX, Wang EZ, et al. Watching dynamic self-assembly of web buckles in strained MoS_2 thin films. *ACS Nano*. 2019;13(3):3106-3116.
72. Wang YL, Cong CX, Qiu CY, Yu T. Raman spectroscopy study of lattice vibration and crystallographic orientation of monolayer MoS_2 under uniaxial strain. *Small*. 2013;9(17):2857-2861.
73. Cai YQ, Lan JH, Zhang G, Zhang YW. Lattice vibrational modes and phonon thermal conductivity of monolayer MoS_2. *Phys Rev B*. 2014;89(3):035438.
74. Rice C, Young RJ, Zan R, et al. Raman-scattering measurements and first-principles calculations of strain-induced phonon shifts in monolayer MoS_2. *Phys Rev B*. 2013;87(8):081307.
75. Yoon D, Son Y-W, Cheong H. Strain-dependent splitting of the double-resonance Raman scattering band in Graphene. *Phys Rev Lett*. 2011;106(15):155502.
76. An CH, Xu ZH, Shen WF, et al. The opposite anisotropic Piezo-resistive effect of ReS_2. *ACS Nano*. 2019;13(3):3310-3319.
77. Feng W, Zheng W, Gao F, et al. Sensitive electronic-skin strain sensor Array based on the patterned two-dimensional α-In_2Se_3. *Chem Mater*. 2016;28(12):4278-4283.
78. Park YJ, Sharma BK, Shinde SM, et al. All MoS_2-based large area, skin-attachable active-matrix tactile sensor. *ACS Nano*. 2019;13(3):3023-3030.
79. Bae GY, Pak SW, Kim D, et al. Linearly and highly pressure-sensitive electronic skin based on a bioinspired hierarchical structural Array. *Adv Mater*. 2016;28(26):5300-5306.
80. Wang Y, Yang T, Lao J, et al. Ultra-sensitive graphene strain sensor for sound signal acquisition and recognition. *Nano Res*. 2015;8(5):1627-1636.
81. Ko KY, Lee S, Park K, et al. High-performance gas sensor using a large-area WS_xSe_{2-X} alloy for low-power operation wearable applications. *ACS Appl Mater Interfaces*. 2018;10(40):34163-34171.
82. Jian MQ, Wang CY, Wang Q, et al. Advanced carbon materials for flexible and wearable sensors. *Sci China Mater*. 2017;60(11):1026-1062.
83. Choi C, Lee Y, Cho KW, Koo JH, Kim D-H. Wearable and implantable soft bioelectronics using two-dimensional materials. *Acc Chem Res*. 2019;52(1):73-81.
84. Akinwande D, Petrone N, Hone J. Two-dimensional flexible nanoelectronics. *Nat Commun*. 2014;5(1):5678.
85. Wang Y, Wang L, Yang TT, et al. Wearable and highly sensitive graphene strain sensors for human motion monitoring. *Adv Funct Mater*. 2014;24(29):4666-4670.
86. Pang Y, Tian H, Tao LQ, et al. Flexible, highly sensitive, and wearable pressure and strain sensors with Graphene porous network structure. *ACS Appl Mater Interfaces*. 2016;8(40):26458-26462.
87. Yao HB, Ge J, Wang CF, et al. A flexible and highly pressure-sensitive Graphene-polyurethane sponge based on fractured microstructure design. *Adv Mater*. 2013;25(46):6692-6698.
88. Chen Z, Ming T, Goulamaly MM, et al. Enhancing the sensitivity of Percolative Graphene films for flexible and transparent pressure sensor arrays. *Adv Funct Mater*. 2016;26(28):5061-5067.
89. Ho DH, Sun Q, Kim SY, Han JT, Kim DH, Cho JH. Stretchable and multimodal all Graphene electronic skin. *Adv Mater*. 2016;28(13):2601-2608.
90. Park M, Park YJ, Chen X, Park Y-K, Kim M-S, Ahn J-H. MoS_2-based tactile sensor for electronic skin applications. *Adv Mater*. 2016;28(13):2556-2562.
91. Guo Y, Zhong MJ, Fang ZW, Wan PB, Yu GH. A wearable transient pressure sensor made with MXene nanosheets for sensitive broad-range human-machine interfacing. *Nano Lett*. 2019;19(2):1143-1150.
92. Choi C, Choi MK, Liu S, et al. Human eye-inspired soft optoelectronic device using high-density MoS_2-graphene curved image sensor array. *Nat Commun*. 2017;8(1):1664.
93. Wang C, Yang SX, Zhang HR, et al. Synthesis of atomically thin GaSe wrinkles for strain sensors. *Front Phys Beijing*. 2016;11(2):116802.
94. Xu MX, Qi JJ, Li F, Zhang Y. Highly stretchable strain sensors with reduced graphene oxide sensing liquids for wearable electronics. *Nanoscale*. 2018;10(11):5264-5271.

AUTHOR BIOGRAPHIES

Hanjun Jiang is a Doctoral candidate in the Institute of Flexible Electronics at Northwestern Polytechnical University (NWPU). He received his BSc degree from School of Life Sciences at NWPU in 2019. His research interests focus on the syntheses of 2D materials and their flexible sensor applications.

Lu Zheng is an associate professor in the Institute of Flexible Electronics at Northwestern polytechnical University, China. She received his Ph.D. from Okayama University, Japan. She worked as research fellow in the school of Materials Science and Engineering at Nanyang Technological

University, Singapore. Her research field is investigation of novel two-dimensional materials their physical properties under extreme condition. She have published more than 20 papers in international journals such as Physical Review B and Journal of Power Sources.

Zheng Liu is an Associate Professor at Nanyang Technological University, Singapore. He works on the synthesis of high-quality and large-size novel 2D monolayers, especially transition metal dichalcogenides (TMDs) and their applications in catalysis and electronics. He has published >200 papers with total citations >20 000 and an H-index of 69. He was the finalist of the World Technology Award in Energy category in 2012. In 2013, he was awarded the prestigious Singapore NRF Fellowship and the elite Nanyang Assistant Professorship. He was awarded ICON-2DMAT Young Scientist Award and the prestigious Singapore Young Scientist Award in 2018. He was the highly cited researcher in 2018 and 2019. He was also named Materials Research Society of Singapore Chair Professorship in 2019.

Xuewen Wang is a Professor in the Institute of Flexible Electronics at Northwestern Polytechnical University, China. He received his PhD in materials science from Nanyang Technological University, Singapore. His research interests are in the area of flexible electronics. He has published 40 papers in prestigious journals such as Science Advances and Advanced Materials, with the total citation of ~2500 times and the H-index is 24. His group devoted to developing in situ and ex situ characterization techniques to reveal the sensing and failure mechanism for flexible materials and flexible sensors.

How to cite this article: Jiang H, Zheng L, Liu Z, Wang X. Two-dimensional materials: From mechanical properties to flexible mechanical sensors. *InfoMat*. 2020;2:1077–1094. https://doi.org/10.1002/inf2.12072